Food Packaging and Shelf Life 23 (2020) 100464

Contents lists available at ScienceDirect

Food Packaging and Shelf Life

journal homepage: www.elsevier.com/locate/fpsl

Cellulose nanofibrils versus cellulose nanocrystals: Comparison of performance in flexible multilayer films for packaging applications

Lu Wang[a,b], Cong Chen[a,b], Jinwu Wang[a,b,c,*], Douglas J. Gardner[a,b], Mehdi Tajvidi[a,b]

[a] Advanced Structures and Composites Center, University of Maine, 35 Flagstaff Road, Orono, ME 04469-5793, USA
[b] School of Forest Resources, University of Maine, 5755 Nutting Hall, Orono, ME 04469-5755, USA
[c] Forest Products Laboratory, U.S. Forest Service, 1 Gifford Pinchot Drive, Madison, Wisconsin 53726, USA

ARTICLE INFO

Keywords:
Cellulose nanomaterials
Gas barrier
Lamination
Adhesive
Transparent film
Hornification

ABSTRACT

Cellulose nanomaterials (CNMs) are a unique type of nanomaterial that are produced via several routes including chemical and mechanical, including the most researched cellulose nanocrystals (CNCs) and cellulose nanofibrils (CNFs). CNM films exhibit excellent oxygen barrier properties in medium to low relative humidity conditions. The oxygen barrier characteristics are desirable for CNM film proposed use in food packaging applications where both performance and biodegradability are of concern. However, the oxygen barrier property of CNM films is reduced if films are exposed to high relative humidity (RH) because of moisture-induced plasticizing and swelling. In this research, CNM films were laminated with polypropylene (PP) film using a polyurethane (PU) adhesive tie layer to form flexible multilayer film packaging. The physical properties of the CNM films indicated that CNC films were denser (~1.4 g/cm^3) than CNF films (1.1–1.3 g/cm^3). Casting weight affected the densities of the CNM films and this effect was material type dependent. Optical property evaluation showed that the CNC films were clearer than the CNF films. Laminating CNF films with PU improved the transparency of the CNF films. Mechanical test results showed that CNC and CNF laminates containing thicker CNM films had similar maximum tensile strength as the control PP/PU laminates. Laminating CNM films with PP and PU significantly improved the barrier properties of the CNM films. For example, the water vapor transmission rate of CNC film dropped from 516 to 1.0 g/(m^2·day). The oxygen transmission rate of CNC film at 80 % RH decreased from 126 to 6.1 cm^3/(m^2·day).

1. Introduction

Appropriate packaging technology is essential for preserving food from deterioration and being disposed of as waste, which accounts for 40 % of all food produced in the USA (Gunders, 2012). To extend the shelf life of food, packaging has to reduce/prevent the transmission of gases from the ambient environment to food, especially oxygen and water vapor which are essential for spoilage microbes to thrive (Wang et al., 2017). Packaging is a large industry segment in the USA and across the world where petroleum-based plastics are used for their excellent performance, easy processing and low price (Rhim, Park, & Ha, 2013). For instance, polypropylene (PP) is low cost packaging material, possessing low water vapor permeability of 7 – 20 g·μm/(m^2·day·kPa) (Lange & Wyser, 2003). However, PP has a high oxygen permeability (OP) of 50-100 cm^3·μm/(m^2·day·kPa), thus is rated as "poor" in oxygen barrier property (Lange & Wyser, 2003; Wang et al., 2017). One industrialized solution to improving the barrier performance of PP is laminating PP with a material of high oxygen barrier property, for example, ethylene vinyl alcohol (EVOH) (Mokwena & Tang, 2012; Wang et al., 2017; Zhang, Britt, & Tung, 2001). However, petroleum-based plastics are not biodegradable, which has caused a huge environmental impact after being discarded in landfills or littered in the oceans. The demand on replacing petroleum-based plastics or at least increasing the amount of biodegradable component in packaging is becoming urgent.

Cellulose nanomaterial (CNM) films, mainly including cellulose nanofibrils (CNFs), cellulose nanocrystals (CNCs) and bacterial cellulose (BC), are reported to display outstanding oxygen barrier properties that are comparable to ethylene vinyl alcohol (EVOH) (Wang et al.,

Abbreviations: CNM, cellulose nanomaterials; CNF, cellulose nanofibrils; CNC, cellulose nanocrystals; BOPP, biaxial-oriented polypropylene; PE, polyethylene; PU, polyurethane; PPL, laminates made by polypropylene and polyurethane; SEM, scanning electron microscope; WVTR, water vapor transmission rate; WVP, water vapor permeability; OTR, oxygen transmission rate; OP, oxygen permeability; RH, relative humidity

* Corresponding author.
E-mail addresses: lu.wang@maine.edu (L. Wang), cong.chen@maine.edu (C. Chen), jinwu.wang@maine.edu, jinwu.wang@usda.gov (J. Wang), douglasg@maine.edu (D.J. Gardner), mehdi.tajvidi@maine.edu (M. Tajvidi).

https://doi.org/10.1016/j.fpsl.2020.100464
Received 25 September 2019; Received in revised form 27 November 2019; Accepted 3 January 2020
Available online 16 January 2020
2214-2894/ Published by Elsevier Ltd.

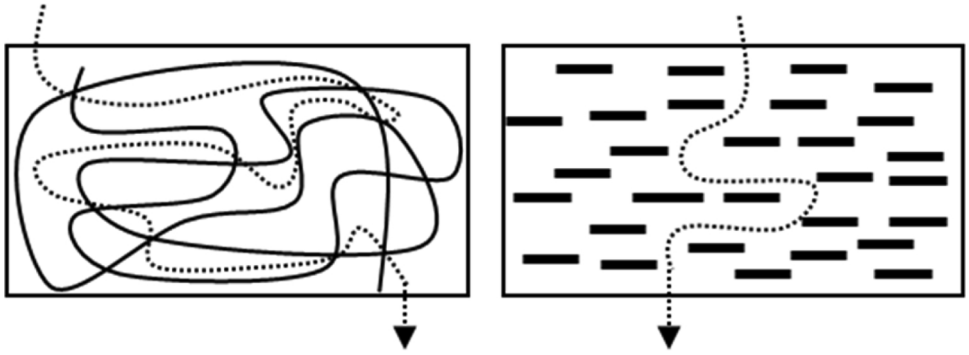

Fig. 1. Scheme of a gas passing through CNF (left) and CNC (right) films via cross sections.

2017). The oxygen barrier property of CNMs remains high at low to medium relative humidity (< 50 % RH) as summarized in several review articles (Azeredo, Rosa, & Mattoso, 2017; Bharimalla, Deshmukh, Vigneshwaran, Patil, & Prasad, 2017; Ferrer, Pal, & Hubbe, 2017; Hubbe et al., 2017; Khalil et al., 2016; Khan, Huq, Khan, Riedl, & Lacroix, 2014; ; Wang et al., 2017). The difference in the polarity between oxygen and CNMs leads to a low solubility of oxygen (Lagaron, Catalá, & Gavara, 2004). Thus, oxygen is not readily adsorbed onto the CNMs surface upon contact. When some oxygen molecules do manage to cross the CNMs surface, they encounter a high-density cohesive energy formed by hydrogen (H) bonding among individual CNMs (Lagaron et al., 2004). The H bonding is strong enough to narrow the gap among CNMs to block gas molecules (Aulin, Gällstedt, & Lindström, 2010). Moreover, to diffuse through CNM films, gases go through a tortuous path created by entanglements/arrangements of CNMs, which is far longer than the thickness of the CNM films (Ferrer et al., 2017). All those characteristics enable CNM films to be extraordinary oxygen barriers. While both CNC and CNF films are excellent oxygen barriers, paths available for gases to diffuse are different depending on their morphological properties. As shown in Fig. 1, CNFs with high aspect ratio can turn and entangle into a web structure, leading to a tortuous diffusion path (Belbekhouche et al., 2011). Meanwhile, in CNCs, uniform and rigid nanofibers can arrange in a more ordered layered structure, imparting CNC films with less voids and higher density (Chowdhury et al., 2018). Whether CNCs or CNFs are better in terms of gas barrier property remains a subject of debate (Wang et al., 2017). In one research paper, gas permeability of CNFs was reported to be lower than CNCs (Belbekhouche et al., 2011). Explanation on why CNFs had a better gas barrier property than CNCs was insufficient as authors pointed out that CNFs had higher density than the CNCs (Belbekhouche et al., 2011). The explanation led to that conclusion was that CNFs contain hemicellulose which lends flexibility to the material, so CNFs were assumed to pack denser than CNCs (Belbekhouche et al., 2011). However, recent publications show that CNC films typically have a density around 1.5 g/cm^3 (Chowdhury et al., 2018; Visanko et al., 2015), while CNF films have a density around 1.1 g/cm^3 (Henriksson, Berglund, Isaksson, Lindstrom, & Nishino, 2008; Kumar et al., 2014; Tayeb & Tajvidi, 2018). A more definitive understanding should be ascertained regarding the oxygen barrier property when comparing CNFs and CNCs.

Moisture, or water vapor, is an important factor negatively impacting the oxygen barrier property of CNMs (Hubbe et al., 2017). Water molecules can disassociate the H bonding formed among CNMs by acting as a plasticizer (Lagaron et al., 2004). The cohesive energy density is lowered and the porosity of the films is enlarged by water (Miettinen, Chinga-Carrasco, & Kataja, 2014). Moisture contributes to the formation of passages between the fibrils or crystals. Thus, oxygen molecules can permeate through these passages with cooperative chain motion of the CNMs (Wang et al., 2017). The poor oxygen barrier property of CNMs in high humidity has contributed to a series of research activities. Applied research approaches include surface modification of the CNMs (Tomé et al., 2010; Visanko et al., 2015), blending CNMs with other materials (Aulin, Salazar-Alvarez, & Lindström, 2012; Liu & Berglund, 2012; Matuana, Karkhanis, Stark, & Sabo, 2016; Tayeb & Tajvidi, 2018), cross-linking the CNMs (Shimizu, Saito, & Isogai, 2016; Tayeb & Tajvidi, 2018), hydrophobic coating (Österberg et al., 2013) and attaching CNM films onto plastic films (Fotie et al., 2017; Mascheroni et al., 2016; Vähä-Nissi et al., 2017; Vartiainen et al., 2016). Most strategies appear to be effective to certain degree towards reducing the oxygen permeation of CNM films at high RH. A detailed list of barrier performance of CNMs films before and after treatment has been reported (Wang et al., 2017). Multilayer packaging where CNM films are used in the core and plastic films as a skin was identified as having great commercial potential in a couple of review articles (Hubbe et al., 2017; Wang et al., 2017). The manufacturing of multilayer packaging films has been a commercial process for decades. If CNMs can replace current oxygen barrier layers, adoption of CNMs in such a process will be easier and faster. However, the oxygen barrier performance of laminates containing CNMs at high RH reported in literature is not sufficient for packaging some food like peanuts and meat (Fotie et al., 2017; Mascheroni et al., 2016; Vähä-Nissi et al., 2017; Vartiainen et al., 2016). Therefore, the further performance enhancements of CNMs in multilayer packaging are needed.

The purpose of this research was to investigate and improve the barrier performance of PP/CNMs/PP multilayer packaging films and compare the performance of CNC and CNF films in multilayer packages. Barrier properties (WVTR, WVP, OTR and OP) were obtained based on the protocols described in American Society for Testing and Materials. Tensile properties of the films were measured. Morphological characteristics of films were obtained using a scanning electron microscope (SEM). Transparency of films was determined by Ultraviolet-Visible Light Spectroscopy (UV-VIS). The results indicated that CNMs can be used in many multilayer food packaging applications for extending the shelf life of food.

2. Experimental section

2.1. Materials

CNMs were supplied by the Process Development Center (PDC) at the University of Maine. CNC suspension was produced at a solids content of 10.3 wt.% at the Forest Products Laboratory of USDA (Madison, WI) from dissolving pulp. Because CNC is produced through sulfuric acid hydrolysis, it contains approximately 300 mmol sulfur per kg measured by ICP-AES. A CNC is about 5 − 20 nm wide and 150 − 200 nm long as shown in Fig. 2 (a). CNFs were produced at the PDC based on a disk refining method from bleached northern softwood kraft pulp (Postek, Moon, Rudie, & Bilodeau, 2013). The solids content of the CNF suspension was 3.0 wt.%. CNF has a nominal fiber width of 50 nm and a length of up to several hundred microns as shown in

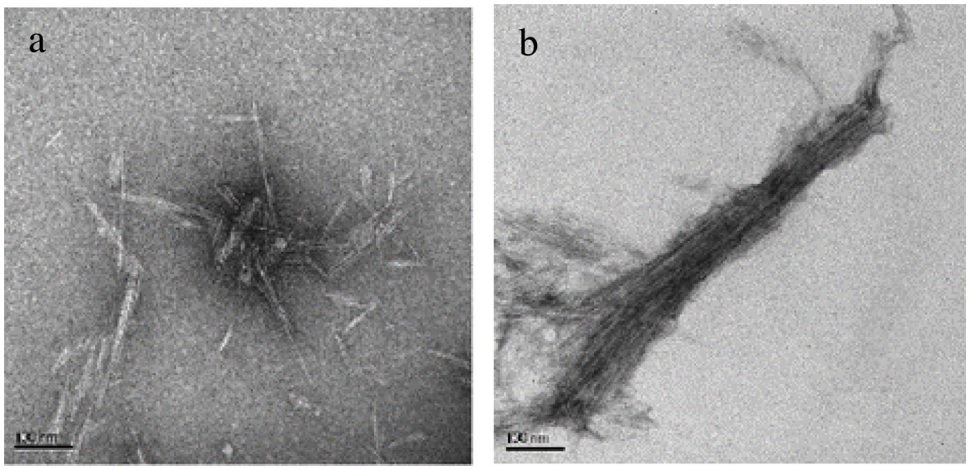

Fig. 2. TEM micrographs of negatively stained CNC (a) and CNF (b) (scale bar: 100 nm. Reproduced from Peng, Gardner, & Han, 2012).

Fig. 2(b). More information about the basic properties of CNMs can be found in this review (Moon, Martini, Nairn, Simonsen, & Youngblood, 2011). D-Sorbitol (> 98 %) was purchased from Sigma-Aldrich to be used as a plasticizer for CNC films. Bi-axial oriented polypropylene (BOPP) films (CLG30) were provided from Treofan Germany GmbH & Co. This film is 30-μm thick, transparent and suitable for lamination. Translucent polyurethane (PU) tie layer films (3231) were supplied by Bemis Associates Inc. (Massachusetts, USA), with a thickness of 50 μm.

2.2. Multilayer film manufacturing

CNM films of two different weights (Table 1) were formed by solution casting CNMs at different solids contents in a polystyrene petri dish (Ø100 mm) and dried in a fume hood at ambient temperature (21 °C). The low level casting weight of 20 g/m^2 was selected because it yielded the minimum thickness for being taken out of petri dish without significant damage to the film sample. The high level casting weight of 50 g/m^2 was chosen based on previous published results where similar thickness was used (Tayeb & Tajvidi, 2018). All suspensions were cast at a total weight of 15 g except CNF50 that was too viscous, thus more water was added for a total weight of 25 g. For the CNC films, 20 wt.% sorbitol based on the total solids weight was added into CNC suspensions to improve flexibility for handling. CNM dry films were conditioned at 50 % RH and 23 °C for at least 24 h. Then the CNM films were laminated with a BOPP film in a HL-200 hot-roll laminator (ChemInstruments, Fairfield, Ohio). PU films were inserted between the CNM films and BOPP films to provide adhesion for the dissimilar interfaces. A structure of BOPP/PU/CNMs/PU/ BOPP film was formed. The lamination pressure was 0.55 MPa, with a temperature of 90 °C and a lamination speed of 60 cm/min. Laminates containing either CNCs or CNFs at different casting weights were labeled as CNC20 L, CNC50 L, CNF20 L and CNF50 L. The BOPP/PU/PU/BOPP laminates (PPL) served as control samples. Multilayer films were then stored in a standard TAPPI room (23 °C and 50 % RH) for future use.

Table 1
Physical properties of cellulose nanomaterials films.

Samples	Casting weight (g/m^2)	Thickness (μm)	Density (g/cm^3)	Porosity (%)
CNC20	20.5 (1.8)[a]	14 (1)	1.43 (0.01)	1.5 (0.6)
CNC50	50.1 (1.9)	36 (2)	1.42 (0.02)	2.2 (1.2)
CNF20	21.4 (3.5)	18 (4)	1.17 (0.07)	21.8 (4.9)
CNF50	51.5 (3.2)	39 (5)	1.31 (0.08)	12.3 (0.1)

[a] values in parenthesis are standard deviations.

2.3. Film characterization

2.3.1. Physical properties of films

Samples with a dimension of 1 cm × 2 cm were cut from the cast films. Densities of the CNM films were calculated based on the ratio of CNM film weight over volume. The porosity of films were calculated from Eq. (1). The ρ is the measured density of a CNM film. The ρ_0 is the real density of CNM materials. For CNC with chiral nematic configuration, ρ_0 was estimated to be 1.45 g/cm^3 (Chowdhury et al., 2018). For CNF, ρ_0 was estimated to be 1.5 g/cm^3 (Henriksson et al., 2008). An environmental scanning electron microscope (ESEM) (TM 3000, Hitachi High-Technologies Corporation, Tokyo, Japan) was used to reveal the low-magnification morphology related to the ruptured cross sections of the CNM laminates after tension tests. High magnification images of the CNM films for higher casting weights were obtained using a field-emission SEM (FESEM) (NVision 40, Zeiss, Germany) at an accelerating voltage of 2 kV to examine fine structural details of the CNMs. An UV–vis spectrometer (USB2000 +, Ocean Optics, FL, USA) with a halogen light source (DH-2000) was used to quantify the transparency of the films to visible light. The device was operated in the transmission mode and air was used as the reference. The transparency of multilayer films was also qualitatively determined by laying films over logos consisting of the Advanced Structures and Composites Center at University of Maine and the USDA-Forest Service Forest Products Laboratory.

$$Porosity = \left(1 - \frac{\rho}{\rho_0}\right) \times 100\% \quad (1)$$

2.3.2. Tensile properties of films

Tensile strength and modulus of elasticity of the multilayer films were determined using an Instron 5942 with a 500 N load capacity. For testing, rectangular specimens of 60 mm × 10 mm were cut from each film. The gap between the tensile test grips was set at 10 mm. The crosshead speed was 2 mm/min. Specimens were tested with at least three replicates and the results were calculated based upon averaged values. A statistical student's test was conducted on the tensile properties.

2.3.3. Barrier properties of films

Water vapor transmission rate (WVTR) and water vapor permeability (WVP) of the multilayer films were obtained according to ASTM E96/E96M-16 Standard Test Methods for Water Vapor Transmission of Materials. A brief description of the procedure is as follows: multilayer film disks with a diameter of 7 cm were obtained using a circle cutter. About 50 g of deionized (D.I.) water was added into a Mason jar of 115 g capacity (Ball, Rubbermaid Incorporated, GA, USA). The film was

laid on the opening of the Mason jar and sealed in place with a silicone-rubber gasket and a metal screw cap. The spatial sequence of the whole assembly from top to bottom was: screw cap/film/gasket/mason jar. Assembled test jars were left in the conditioning room for a week (first day was conditioning day) and weighed at Day 1, 2, 3 and 7. WVTR and WVP were calculated using following equations:

$$WVTR = (G/t)/A \quad (2)$$

Where: G is the weight (g), t is the time (d), G/t is the slope of the linear portion of weight change and A is the test area (the cup mouth area, m^2);

$$WVP = WVTR * d/S(R_1 - R_2) \quad (3)$$

Where: S is the saturation vapor pressure at the test temperature (2.81 kPa at 23 °C), R_1 is the relative humidity inside the Mason jar (100 %) and R_2 is the relative humidity of the testing environment (50 %) and d is the film thickness (μm). All samples were tested with one replicate and both values were reported.

Oxygen transmission rate (OTR) and oxygen permeability (OP) of the multilayer films were measured using an oxygen permeation analyzer (OX-TRAN® Model 2/22 L, MOCON, Minneapolis, MN, USA) according to ASTM F1927 Standard Test Method for Determination of Oxygen Gas Transmission Rate, Permeability and Permeance at Controlled Relative Humidity Through Barrier Materials Using a Coulometric Detector. Film samples were first masked by aluminum foil to give a test area of 5 cm^2 and then placed between two chambers at ambient atmospheric pressure. One chamber was purged with nitrogen at a 23 °C and 80 % RH. The other chamber was purged with oxygen at the same temperature and relative humidity. After oxygen transmits into the nitrogen stream, it was sent to a coulometric detector to determine the amount of oxygen. The end of tests was determined based on a convergence method. That is, in a total of 5 testing cycles (each lasting about 1 h), if the variation between two adjacently detected OTRs was smaller than 1 %, then the test was concluded. The OTR and OP values were automatically calculated by the build-in software of the analyzer. All films and D.I. water were conditioned in the conditioning room for at least 24 h before gas transmission tests. Samples were tested in duplicate. A student's test was conducted on the results.

3. Results and discussion

3.1. Physical properties of CNM films

The physical properties of the CNM films of different types and thickness are shown in Table 1. The CNC films have a higher density and lower porosity than the CNF films. One of the reasons is that the CNCs have "rice-like" structure while the CNFs have "spaghetti-like" structure (Wang, Sanders, Gardner, & Han, 2016). CNCs can pack more densely than the CNFs attributed to their homogenous dimensions. The effect of casting weight on the densities of CNM films varies by the material type. For CNCs, casting weight does not appear to affect the density (Table 1). For CNFs, higher the casting weight, larger the film density. When dried, CNF20 films are smoother and much less wrinkled than the CNF50 films. The wrinkling of the CNF50 films originates from the fact that the interfacial adhesion force between the polystyrene petri-dish and CNF films is weaker than the internal shrinking force of CNF films during drying. Because the fibrils can get closer together, instead of being fixed on certain locations on the petri-dish, film porosity is reduced and density is increased for CNF50.

Higher magnification micrographs of CNM films are shown in Fig. 3. Upon visual inspection (not shown), CNC20 and CNC50 films both display iridescence colors attributed to their chiral nematic liquid crystal structures (Bardet, Belgacem, & Bras, 2015). The layered liquid crystal structure of CNC is verified in Fig. 3. The pitch length of the CNC50 films varies by location because film thickness is not even. Many nanoscale pores exist when observing the surface of the CNM films. The pores are created by bridging occurring among the nanofibers. CNC50 film has a smoother surface with all pores similar in size, while the CNF50 film possesses a great disparity in pore size. There are also possibly vacant sites in the CNF50 film created by trapped air.

Fig. 4a shows the transmittance of the studied films measured with a UV–vis spectrometer. PP alone is the most transparent film, followed by the CNC-containing films. The CNF films are opaque because their surface pores greatly scatter visible light (Nogi, Iwamoto, Nakagaito, & Yano, 2009). Laminating with translucent PU films significantly reduces the transparency of PP and CNC films, while slightly improving the transparency of the CNF films. CNF films can be made more transparent by laminating with polycarbonate film (Nogi et al., 2009). Plastic film can smooth the surface of CNF films, thus reducing the light scattering and improving transparency (Nogi et al., 2009). When the CNM film layers become thicker, the films, as well as their corresponding laminates become less transparent (Kiziltas, Kiziltas, Bollin, & Gardner, 2015). A classic, quick and qualitative way to evaluate the optical transparency of CNM films is to lay films over objects (Kiziltas et al., 2015;). The size of the films is roughly indicated with blue dash line circles in Fig. 4b. These circles assist with differentiating the change in clearness between objects covered with films (inside circles) and objects not covered with films (outside circles). The darker one of the two logos (Advanced Structures and Composites Center at the University of Maine) provides better contrast (red arrow). Similar conclusions can be drawn here regarding the transparency of different samples.

In summary, CNC films outperform CNF films in transparency.

3.2. Tensile property of films

Sufficient mechanical properties are basic criteria for a material used in load bearing applications. For flexible food packaging, the stiffness or elastic modulus is less of a concern than strength. The tensile strength of CNC and CNF films are shown in Fig. 5.

The average tensile strength and elastic modulus of the CNC films was around 63 MPa and 6.8 GPa, close to what has been reported for CNC films in the literature (Bardet et al., 2015; Nan et al., 2017; Visanko et al., 2015). The tensile stress and modulus of the CNF50 films was around 110 MPa and 2.9 GPa, which also aligns with previously reported values (Benítez & Walther, 2017; Kumar et al., 2014; Tayeb & Tajvidi, 2018). Generally, CNC films are weaker than CNF films. One evident reason is attributed to the sorbitol, a plasticizer that lowers the tensile strength of the CNC films (Bardet et al., 2015). Another reason is that CNC films do not achieve the same degree of flexibility as CNF films. The CNC/sorbitol films are still prone to cracking from defects, resulting in early failure. However, CNC films are stiffer than CNF films because of a higher density and crystallinity (Claro et al., 2019). The CNF20 films are weaker and softer than the CNF50 films because the latter is much denser (Table 1). Smaller porosity in CNF50 films helps increase their mechanical properties (Benítez & Walther, 2017). CNC20 and CNC50 films are similar in tensile properties attributed to their small density differences (Table 1).

Both the CNC20 L and CNF20 L films exhibit lower tensile strength than any individual component comprising the laminates, e.g. CNC20 films, CNF20 films or PPL films. The reason for this is not completely clear. One assumption is that the applied lamination pressure was too high. High pressure potentially weakened the film strength because films were thin at low casting weight. Although the CNF50 films have much higher strength than the PPL films, the CNF50 films slightly improved the strength of PPL films after incorporation into the laminated composite structure. A similar trend was reported for polyhydroxyalkanoates (PHA) coated CNF films (Cherpinski et al., 2018). It was determined that the tensile strength of the layered films remained the same as the base plastic films. If CNM films are stronger than the plastic skin layers, the tension failure will still occur in the plastic layers. The same theory also applies to the elastic modulus change of materials

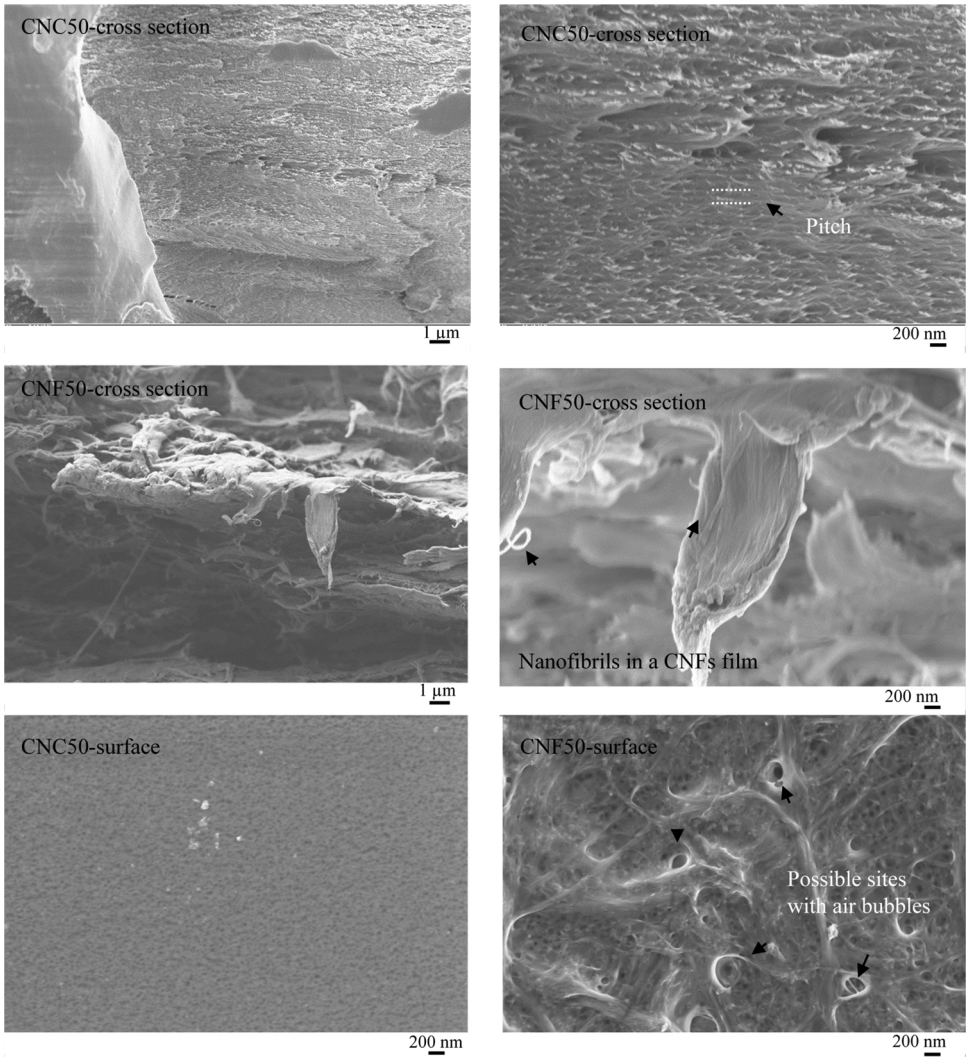

Fig. 3. FESEM graphs of the cross sections and surface of CNM films.

after being laminated. Our study, therefore, does not show that CNM films are enhancements for the tensile properties of plastic films.

Morphology of the ruptured surface of the films after the tensile testing is shown in Fig. 6. PP films are incompressible during lamination as their thickness does not appear to change much. PU films are densified during lamination. PU does not penetrate deeply into the CNM films. During the tension tests, the PU debonds at the interfaces and displays plastic deformation. Both the PPL and CNC films have clear ruptured surfaces, which indicates a brittle fracture. The CNF films show rough surfaces with fibers pulled out. Though strain values are not reliable thus not reported, those morphological features imply that the PU and CNFs may improve the toughness of the laminates.

In summary, the CNC and CNF films performed similarly in terms of tensile properties of the multilayer packaging films when of similar thickness. The thicker CNM films render higher tensile strength to laminates than the thinner. However, flexible CNF films are better for handling than brittle CNC films.

3.3. Barrier properties of films

3.3.1. Water vapor barrier properties

Because CNM films are sensitive to moisture absorption, the water vapor barrier property is an important measurement for efforts aimed at improving the gas barrier properties of CNM films. Previous research has discovered that CNM films are hygroscopic with high WVTR and laminating CNM films with moisture barrier polymers significantly reduced the WVTR and WVP of CNM films (Cherpinski et al., 2018; Vähä-Nissi et al., 2017). All laminates in Table 2 are classified as high water vapor barrier materials (Wang et al., 2017). As shown in Table 2, the WVTR of all CNM laminates are below 1.0 g/(m^2·day). For comparison, the WVTR values of the CNF/LDPE layered films manufactured in a similar fashion were reported to be 1.6 g/(m^2·day) or 2.0 g/(m^2·day) (Vähä-Nissi et al., 2017; Vartiainen et al., 2016). Material type and thickness of the CNM films do not appear to affect the WVTR of laminates, which was also reflected in a recent publication (Koppolu et al., 2019).

As for plant-based CNM films, the WVTR values are comparable to previous findings (Visanko et al., 2015; Wang et al., 2017). The CNF film (408 − 497 g/(m^2·day)) alone appears to be a better water vapor barrier than the CNC film (452 − 516 g/(m^2·day)). The most important reason is that the tortuous path of CNF films can retard water vapor transmission to a larger extent than CNC films (Fig. 1). Another reason is the addition of sorbitol, a plasticizer, can reduce the H bond density within CNCs, thus increasing moisture transmission (Hubbe et al., 2017). CNM all experience hornification, a process that generates irreversible hydrogen bonding during drying (Hult, Larsson, & Iversen, 2001). Hornification is an important factor improving the barrier properties of CNF films (Österberg et al., 2013). However, the effect of hornification on the barrier properties of CNC films is sparsely reported in the literature. So, it is difficult to compare the degree of hornificaiton

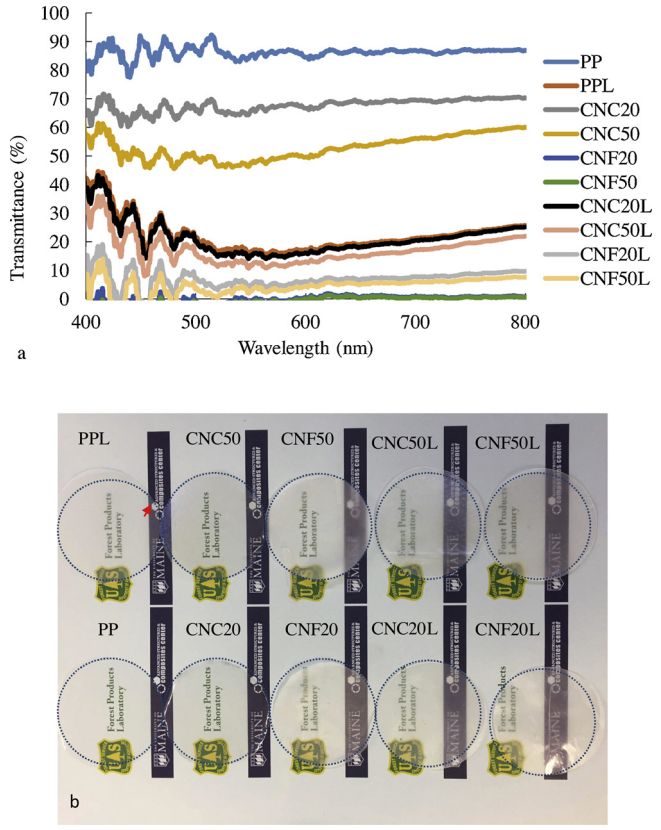

Fig. 4. UV–vis spectrums of films (a) and visual evaluation of the transparency of films (b).

between CNF and CNC films (Ding et al., 2019). Possibly, CNF films possess less degree of hornificaiton than CNC films because the hemicellulose component can prevent direct contact between the cellulose surfaces during drying (Hult et al., 2001). Therefore, the difference in the moisture barrier properties between CNC and CNF films is less likely caused by the amount of hornification.

For CNFs, the greater the film thickness, the lower the WVTR. A similar conclusion was found for paperboard coated with CNFs of various thicknesses (Kumar, Elfving, Koivula, Bousfield, & Toivakka, 2016). Film thickness of CNCs caused less difference in WVTR possibly because of their marginal density differences.

3.3.2. Oxygen barrier properties

Much research had previously proved the excellent oxygen barrier properties of CNM films at a RH level lower than 50 %. So, this study only focused on the oxygen barrier properties of CNM film at 80 % RH (Table 3). Since PU is not a good oxygen barrier layer, laminating PU onto PP does not upgrade the poor oxygen barrier performance of PP (Shamini & Yusoh, 2014). There is little reported on the oxygen barrier properties of single CNC films at high RH possibly because it is difficult to achieve flexible single CNCs films for completing the test. One research paper reported the OP of a bacterial cellulose nanocrystals films to be 507 cm^3·μm/(m^2·day·kPa) at 24 °C and 80 % RH (Martínez-Sanz, Lopez-Rubio, & Lagaron, 2013). Another research paper reported the OP of an amino-modified CNC film to be 5.7 cm^3·μm/(m^2·day·kPa) at 24 °C and 80 % RH (Visanko et al., 2015). Our OP values for CNC films fall between these two research findings. The thicker the CNM films, lower the OTR values of those films attributed to a longer diffusion path. CNF films are better oxygen barriers than the CNC films at high RH because of more tortuous paths created inside CNF films (Fig. 1).

Data from this study demonstrate that CNM films are classified as "low/medium" grade oxygen barrier materials at 80 % RH (Wang et al., 2017). Once CNM films are laminated with PP, their oxygen barrier properties at 80 % RH can be improved. The OTR of laminates containing CNCs were reduced by up to 20 times compared to CNC films. The OTR of laminates containing CNFs were reduced by up to 3 times compared to CNF films. The OTR at 80 % RH of CNM laminates in this study is unprecedentedly low, i.e. 5.7 cm^3/(m^2·day). A previously reported OTR of a HDPE/CNFs/LDPE laminate was 490 cm^3/(m^2·day) at 23 °C and 80 % RH (Vartiainen et al., 2016). A hydrophobic adhesive layer was missing in some studies where plastic skin layers were directly extrusion-coated on CNMs layers (Fotie et al., 2017; Mascheroni et al., 2016; Vähä-Nissi et al., 2017; Vartiainen et al., 2016). It appears that an adhesive layer is essential in integrating all layers into a robust composite structure. As shown in Fig. 3, the surface of the CNM films contains many pores. Without a soft adhesive layer to plug those pores, water vapor can easily disassociate the weak adhesion at the PP/CNMs interface and diffuse into the CNM films as shown in Fig. 7. An adhesive layer can reduce the area penetrated by water vapor, therefore, limiting the water-vapor induced swelling and preserve CNM films as good oxygen barriers at high RH. The decrease in OP of laminates containing CNM films is not as large as those in OTR. The major reason is the use of thick (50 μm) adhesive layers during lamination. The barrier properties of CNM-containing laminates can be further promoted to "high" grade level (< 4 cm^3·μm/(m^2·day·kPa)) if thinner (10 μm) plastic and adhesive layers are used. The excellent oxygen barrier properties of CNM laminates will qualify the use of such films in a majority of food packaging applications including instant coffee, peanuts, meat and potato chips (Wang et al., 2017).

In conclusion, CNF and CNC films in multilayer packaging functioned similarly in resisting water vapor and oxygen transmission. CNCs seem to provide more consistent (smaller standard deviation) and lower OTR values than CNFs.

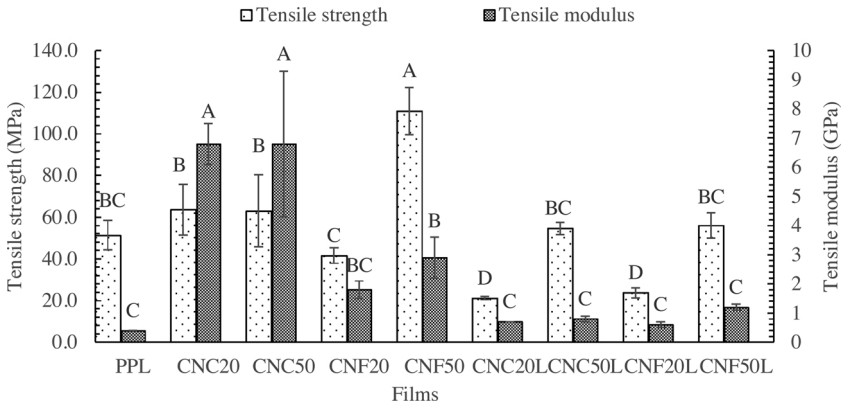

Fig. 5. Tensile properties of the CNC, CNF and laminate films.

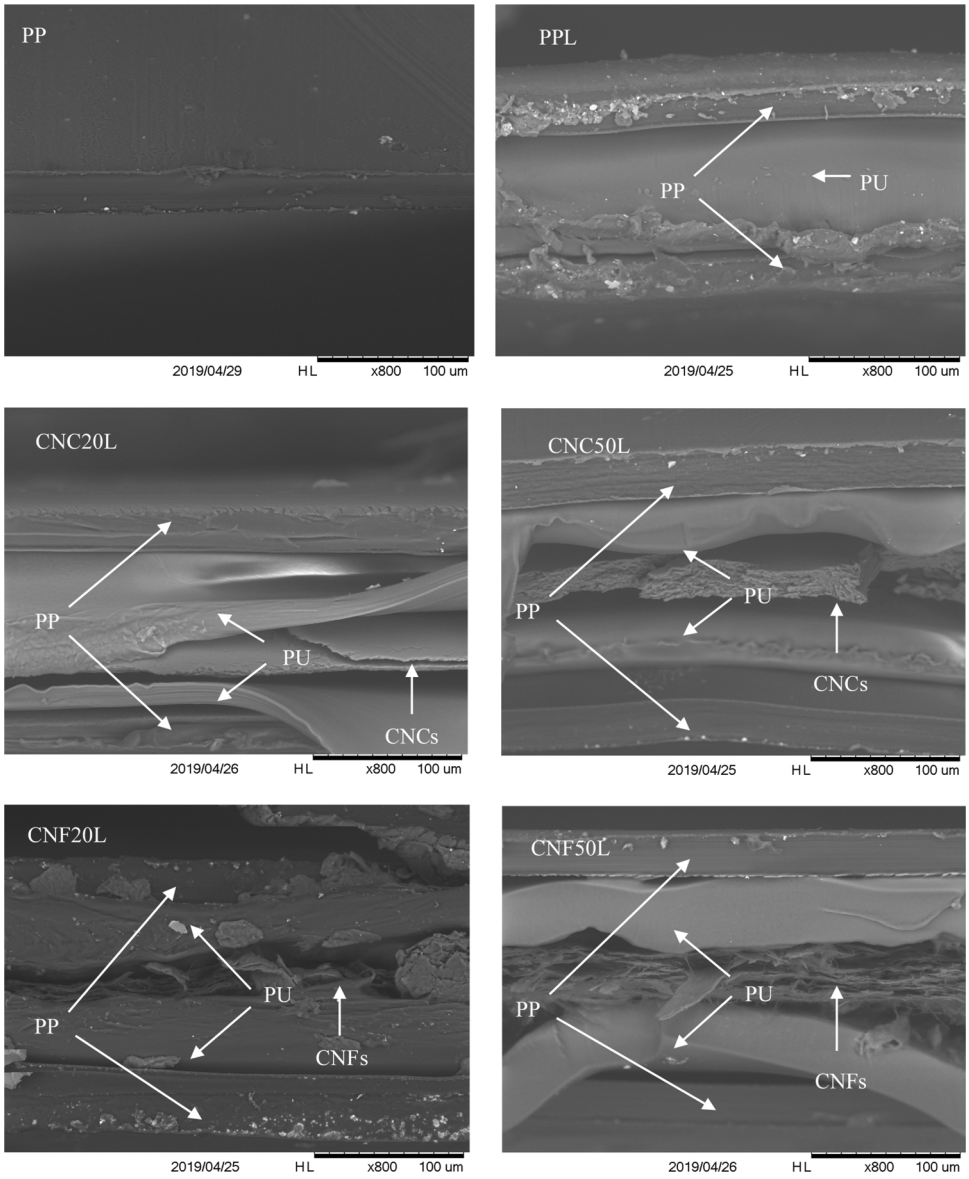

Fig. 6. ESEM graphs of the cross sections of the CNC and CNF films after tensile testing.

Table 2
Water vapor barrier properties of CNM films and their laminates.

Samples	Water vapor transmission rate g/(m²·day)		Water vapor permeability g·μm/(m²·day·kPa)	
PPL	0.6 (0.4)[a]	D[b]	45.5 (20.5)	C
CNC20	515.9 (33.5)	A	4741.5 (729.0)	B
CNC50	452.0 (4.6)	B	12224.5 (785.6)	A
CNF20	497.1 (34.4)	A	5529.5 (1631.3)	B
CNF50	407.6 (33.0)	C	11318.0 (916.4)	A
CNC20L	1.0 (0.1)	D	83.5 (6.4)	C
CNC50L	0.9 (0)	D	82.0 (0)	C
CNF20L	1.0 (0.1)	D	111.5 (10.6)	C
CNF50L	0.8 (0)	D	106.0 (2.8)	C

[a] values in parenthesis are standard deviations.
[b] capital letters represent statistical differences. Values with different letters are significantly different.

Table 3
Oxygen barrier properties of CNM films and their laminates (23 °C, 80 % RH).

Samples	Oxygen transmission rate (cm³/m²·day)		Oxygen permeability (cm³·μm/m²·day·kPa)	
PPL	238.6 (46.7)[a]	A[b]	376.4 (76.9)	A
CNC20	126.4 (25.2)	B	19.3 (3.9)	B
CNC50	55.2 (12.2)	C	20.0 (4.5)	B
CNF20	65.8 (18.3)	C	13.4 (1.9)	B
CNF50	31.3 (5.4)	CD	11.1 (0.9)	B
CNC20L	6.1 (1.1)	D	10.4 (1.9)	B
CNC50L	5.7 (2.1)	D	10.4 (2.0)	B
CNF20L	24.3 (3.5)	CD	42.2 (6.1)	B
CNF50L	10.5 (8.7)	D	18.8 (15.7)	B

[a] Values in parenthesis are standard deviations.
[b] Capital letters represent statistical differences. Values with different letters are significantly different.

4. Conclusions and future work

In this study, the performance of CNC and CNF films were evaluated and compared as free-standing films and in the form of laminates. Although neat CNC films and CNF films have different physical and mechanical properties, their lamination with polymers results in

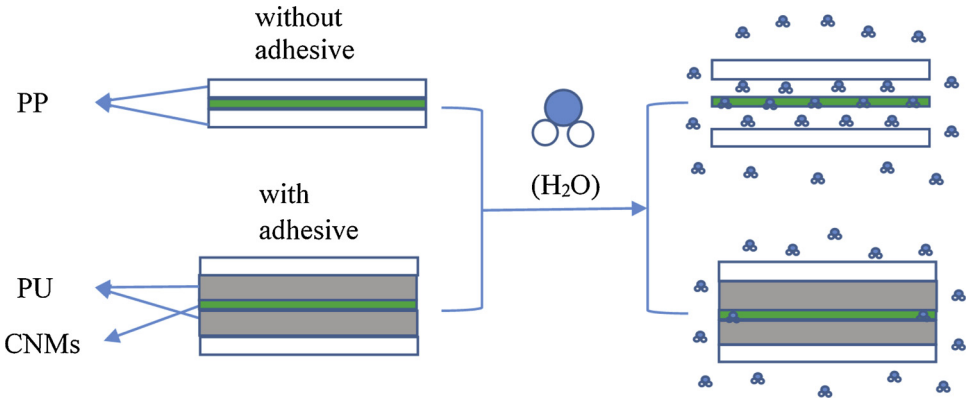

Fig. 7. A scheme explaining how an adhesive layer protects CNM films from being swollen by moisture.

multilayer laminates with similar performance in mechanical and barrier properties but with slightly different transparency. The overall conclusions from this study are summarized below.

1 CNC and CNF films contributed similarly to the water vapor and oxygen barrier properties of the BOPP films. CNC provided better performance consistency than CNF. Lamination greatly improved the water vapor and oxygen barrier properties of the CNM films to an extent that the laminates are classified as high water vapor barriers.
2 CNC films did not greatly impact the transparency of plastic films after lamination. CNF films and their laminates are quite opaque if put away from packaged objects. Laminating CNF films with clear adhesive can further improve its transparency.
3 CNF films are easier to handle than the brittle CNC films. The thickness of CNM films affected the mechanical behavior of the multilayer films. The thicker CNM films rendered higher tensile properties to laminates than the thinner films. Our results confirmed previous findings from other research groups.

Future work following this research includes:

1 Laminate CNM films with biodegradable polymers like polylactic acid (PLA) and measure their properties for packaging applications.
2 Conduct more characterizations on the films for food packaging, i.e. antimicrobial study.
3 Investigate a pilot-scale manufacturing method for producing such laminates.

Funding sources

The research was supported by the USDA-NIFA Agriculture and Food Research Initiative program under grant number of 2018-67010-27906.

CRediT authorship contribution statement

Lu Wang: Methodology, Investigation, Data curation, Visualization, Formal analysis, Writing - original draft. **Cong Chen:** Investigation, Data curation. **Jinwu Wang:** Conceptualization, Funding acquisition, Methodology, Supervision, Writing - review & editing. **Douglas J. Gardner:** Funding acquisition, Project administration, Methodology, Resources, Writing - review & editing. **Mehdi Tajvidi:** Resources, Writing - review & editing.

Acknowledgements

Authors like to express their gratitude to Dr. Colleen Walker, the Director of Process Development Center at the University of Maine for the use of their TAPPI conditioning room and Dr. Ling Li from School of Forest Resources at the University of Maine for the use of her hot press during adhesive selection.

References

Aulin, C., Gällstedt, M., & Lindström, T. (2010). Oxygen and oil barrier properties of microfibrillated cellulose films and coatings. *Cellulose, 17*(3), 559–574.
Aulin, C., Salazar-Alvarez, G., & Lindström, T. (2012). High strength.; flexible and transparent nanofibrillated cellulose–nanoclay biohybrid films with tunable oxygen and water vapor permeability. *Nanoscale, 4*(20), 6622–6628.
Azeredo, H. M., Rosa, M. F., & Mattoso, L. H. C. (2017). Nanocellulose in bio-based food packaging applications. *Industrial Crops and Products, 97*, 664–671.
Bardet, R., Belgacem, N., & Bras, J. (2015). Flexibility and color monitoring of cellulose nanocrystal iridescent solid films using anionic or neutral polymers. *ACS Applied Materials & Interfaces, 7*(7), 4010–4018.
Belbekhouche, S., Bras, J., Siqueira, G., Chappey, C., Lebrun, L., Khelifi, B., et al. (2011). Water sorption behavior and gas barrier properties of cellulose whiskers and microfibrils films. *Carbohydrate Polymers, 83*(4), 1740–1748.
Benítez, A. J., & Walther, A. (2017). Cellulose nanofibril nanopapers and bioinspired nanocomposites: A review to understand the mechanical property space. *Journal of Materials Chemistry A, 5*(31), 16003–16024.
Bharimalla, A. K., Deshmukh, S. P., Vigneshwaran, N., Patil, P. G., & Prasad, V. (2017). Nanocellulose-polymer composites for applications in food packaging: Current status, future prospects and challenges. *Polymer-plastics Technology and Engineering, 56*(8), 805–823.
Cherpinski, A., Torres-Giner, S., Vartiainen, J., Peresin, M. S., Lahtinen, P., & Lagaron, J. M. (2018). Improving the water resistance of nanocellulose-based films with polyhydroxyalkanoates processed by the electrospinning coating technique. *Cellulose, 25*(2), 1291–1307.
Chowdhury, R. A., Nuruddin, M., Clarkson, C., Montes, F., Howarter, J., & Youngblood, J. P. (2018). Cellulose nanocrystal (CNC) coatings with controlled anisotropy as high-performance gas barrier films. *ACS Applied Materials & Interfaces, 11*(1), 1376–1383.
Claro, P., Campos, A., Corrêa, A., Rodrigues, V., Luchesi, B., Silva, L., et al. (2019). Curaua and eucalyptus nanofiber films by continuous casting: Mixture of cellulose nanocrystals and nanofibrils. *Cellulose, 26*(4), 2453–2470.
Ding, Q., Zeng, J., Wang, B., Tang, D., Chen, K., & Gao, W. (2019). Effect of nanocellulose fiber hornification on water fraction characteristics and hydroxyl accessibility during dehydration. *Carbohydrate Polymers, 207*, 44–51.
Ferrer, A., Pal, L., & Hubbe, M. (2017). Nanocellulose in packaging: Advances in barrier layer technologies. *Industrial Crops and Products, 95*, 574–582.
Fotie, G., Rampazzo, R., Ortenzi, M., Checchia, S., Fessas, D., & Piergiovanni, L. (2017). The effect of moisture on cellulose nanocrystals intended as a high gas barrier coating on flexible packaging materials. *Polymers, 9*(9), 415.
Gunders, D. (2012). *Wasted: How America is losing up to 40% of its food from farm to fork to landfill.* Natural Resources Defense Council. Last day of acess: 7/11/19 https://www.nrdc.org/resources/wasted-how-america-losing-40-percent-its-food-farm-fork-landfill.
Henriksson, M., Berglund, L. A., Isaksson, P., Lindstrom, T., & Nishino, T. (2008). Cellulose nanopaper structures of high toughness. *Biomacromolecules, 9*(6), 1579–1585.
Hubbe, M. A., Ferrer, A., Tyagi, P., Yin, Y., Salas, C., Pal, L., et al. (2017). Nanocellulose in thin films, coatings, and plies for packaging applications: A review. *BioResources, 12*(1), 2143–2233.
Hult, E. L., Larsson, P. T., & Iversen, T. (2001). Cellulose fibril aggregation—An inherent property of kraft pulps. *Polymer, 42*(8), 3309–3314.
Khalil, H. A., Davoudpour, Y., Saurabh, C. K., Hossain, M. S., Adnan, A. S., Dungani, R., et al. (2016). A review on nanocellulosic fibres as new material for sustainable packaging: Process and applications. *Renewable and Sustainable Energy Reviews, 64*, 823–836.
Khan, A., Huq, T., Khan, R. A., Riedl, B., & Lacroix, M. (2014). Nanocellulose-based composites and bioactive agents for food packaging. *Critical Reviews in Food Science*

and Nutrition, 54(2), 163–174.
Kiziltas, E. E., Kiziltas, A., Bollin, S. C., & Gardner, D. J. (2015). Preparation and characterization of transparent PMMA–cellulose-based nanocomposites. *Carbohydrate Polymers, 127*, 381–389.
Koppolu, R., Lahti, J., Abitbol, T., Swerin, A., Kuusipalo, J., & Toivakka, M. (2019). Continuous processing of Nanocellulose and polylactic acid into multilayer barrier coatings. *ACS Applied Materials & Interfaces, 11*(12), 11920–11927.
Kumar, V., Bollström, R., Yang, A., Chen, Q., Chen, G., Salminen, P., et al. (2014). Comparison of nano-and microfibrillated cellulose films. *Cellulose, 21*(5), 3443–3456.
Kumar, V., Elfving, A., Koivula, H., Bousfield, D., & Toivakka, M. (2016). Roll-to-roll processed cellulose nanofiber coatings. *Industrial & Engineering Chemistry Research, 55*(12), 3603–3613.
Lagaron, J. M., Catalá, R., & Gavara, R. (2004). Structural characteristics defining high barrier properties in polymeric materials. *Materials Science and Technology, 20*(1), 1–7.
Lange, J., & Wyser, Y. (2003). Recent innovations in barrier technologies for plastic packaging—A review. *Packaging Technology and Science, 16*(4), 149–158.
Liu, A., & Berglund, L. A. (2012). Clay nanopaper composites of nacre-like structure based on montmorrilonite and cellulose nanofibers—Improvements due to chitosan addition. *Carbohydrate Polymers, 87*(1), 53–60.
Martínez-Sanz, M., Lopez-Rubio, A., & Lagaron, J. M. (2013). High-barrier coated bacterial cellulose nanowhiskers films with reduced moisture sensitivity. *Carbohydrate Polymers, 98*(1), 1072–1082.
Mascheroni, E., Rampazzo, R., Ortenzi, M. A., Piva, G., Bonetti, S., & Piergiovanni, L. (2016). Comparison of cellulose nanocrystals obtained by sulfuric acid hydrolysis and ammonium persulfate, to be used as coating on flexible food-packaging materials. *Cellulose, 23*(1), 779–793.
Matuana, L. M., Karkhanis, S. S., Stark, N. M., & Sabo, R. C. (2016). Cellulose nanocrystals as barrier performance enhancer of extrusion-blown PLA films for food applications. *Proceedings*.
Miettinen, A., Chinga-Carrasco, G., & Kataja, M. (2014). Three-dimensional microstructural properties of nanofibrillated cellulose films. *International Journal of Molecular Sciences, 15*(4), 6423–6440.
Mokwena, K. K., & Tang, J. (2012). Ethylene vinyl alcohol: A review of barrier properties for packaging shelf stable foods. *Critical Reviews in Food Science and Nutrition, 52*(7), 640–650.
Moon, R. J., Martini, A., Nairn, J., Simonsen, J., & Youngblood, J. (2011). Cellulose nanomaterials review: Structure, properties and nanocomposites. *Chemical Society Reviews, 40*(7), 3941–3994.
Nan, F., Nagarajan, S., Chen, Y., Liu, P., Duan, Y., Men, Y., et al. (2017). Enhanced toughness and thermal stability of cellulose nanocrystal iridescent films by alkali treatment. *ACS Sustainable Chemistry & Engineering, 5*(10), 8951–8958.
Nogi, M., Iwamoto, S., Nakagaito, A. N., & Yano, H. (2009). Optically transparent nanofiber paper. *Advanced Materials, 21*(16), 1595–1598.
Österberg, M., Vartiainen, J., Lucenius, J., Hippi, U., Seppälä, J., Serimaa, R., et al. (2013). A fast method to produce strong NFC films as a platform for barrier and functional materials. *ACS Applied Materials & Interfaces, 5*(11), 4640–4647.
Peng, Y., Gardner, D. J., & Han, Y. (2012). Drying cellulose nanofibrils: In search of a suitable method. *Cellulose, 19*(1), 91–102.
Postek, M. T., Moon, R. J., Rudie, A. W., & Bilodeau, M. A. (2013). *Production and applications of cellulose*. Peachtree Corners: Tappi Press.
Rhim, J. W., Park, H. M., & Ha, C. S. (2013). Bio-nanocomposites for food packaging applications. *Progress in Polymer Science, 38*(10–11), 1629–1652.
Shamini, G., & Yusoh, K. (2014). Gas permeability properties of thermoplastic polyurethane modified clay nanocomposites. *International Journal of Chemical Engineering and Applications, 5*(1), 64.
Shimizu, M., Saito, T., & Isogai, A. (2016). Water-resistant and high oxygen-barrier nanocellulose films with interfibrillar cross-linkages formed through multivalent metal ions. *Journal of Membrane Science, 500*, 1–7.
Tayeb, A. H., & Tajvidi, M. (2018). Sustainable barrier system via self-assembly of colloidal montmorillonite and cross-linking resins on nanocellulose interfaces. *ACS Applied Materials & Interfaces, 11*(1), 1604–1615.
Tomé, L. C., Brandão, L., Mendes, A. M., Silvestre, A. J., Neto, C. P., Gandini, A., et al. (2010). Preparation and characterization of bacterial cellulose membranes with tailored surface and barrier properties. *Cellulose, 17*(6), 1203–1211.
Vähä-Nissi, M., Koivula, H. M., Räisänen, H. M., Vartiainen, J., Ragni, P., Kenttä, E., et al. (2017). Cellulose nanofibrils in biobased multilayer films for food packaging. *Journal of Applied Polymer Science, 134*(19), https://doi.org/10.1002/app.44830.
Vartiainen, J., Shen, Y., Kaljunen, T., Malm, T., Vähä-Nissi, M., Putkonen, M., et al. (2016). Bio-based multilayer barrier films by extrusion, dispersion coating and atomic layer deposition. *Journal of Applied Polymer Science, 133*(2), https://doi.org/10.1002/app.42260.
Visanko, M., Liimatainen, H., Sirviö, J. A., Mikkonen, K. S., Tenkanen, M., Sliz, R., et al. (2015). Butylamino-functionalized cellulose nanocrystal films: Barrier properties and mechanical strength. *RSC Advances, 5*(20), 15140–15146.
Wang, L., Sanders, J. E., Gardner, D. G., & Han, Y. (2016). In-situ modification of cellulose nanofibrils by organosilanes during spray drying. *Industrial Crops and Products, 93*, 129–135.
Wang, J., Gardner, D. J., Stark, N. M., Bousfield, D. W., Tajvidi, M., & Cai, Z. (2017). Moisture and oxygen barrier properties of cellulose nanomaterial-based films. *ACS Sustainable Chemistry & Engineering, 6*(1), 49–70.
Zhang, Z., Britt, I. J., & Tung, M. A. (2001). Permeation of oxygen and water vapor through EVOH films as influenced by relative humidity. *Journal of Applied Polymer Science, 82*(8), 1866–1872.